ECA Filter Effects on Ground Clutter Statistics in DVB-T Based Passive Radar

Nerea del-Rey-Maestre, María-Pilar Jarabo-Amores, José-Luis Bárcena-Humanes, David Mata-Moya, and Pedro Gómez-del-Hoyo
Signal Theory and Communications Department
Polytechnic School, University of Alcalá
28805 - Alcalá de Henares, Madrid (Spain)
Email: {nerea.rey,mpilar.jarabo,jose.barcena,david.mata,pedrojose.gomez}@uah.es

***Abstract*—This paper tackles the analysis of the Extensive CAncellation (ECA) filter effects in the statistical characterization of ground radar clutter. Real radar databases acquired by a DVB-T based Passive Radar (PR) system were characterized considering the Cross-Ambiguity Function output as the observation space. Goodness-of-fit tests were applied, and skewness and kurtosis values were estimated. The Gaussian model was proved to be suitable for high Doppler shifts. However, Mixture of Gammas and Gaussians distributions were proposed to model the intensity and the in-phase and quadrature components, respectively, of the region centred in the zero Doppler line. These results prove that, although the ECA filter rejects the most part of the interference components, a non-homogeneous characterization was required for Doppler shifts close to zero, where ground clutter effects concentrate. The proposed theoretical distributions will be useful for the formulation of optimum detectors based on the Neyman-Pearson criterion, improving the detection performance of PR systems.**

I. Introduction

Passive Radars (PRs) use non-cooperative signals as illumination sources, Illuminators of Opportunity (IoOs), rather than a dedicated transmitter [1]. PBRs present many advantages against active radars: low development, implementation and computational cost due to the possibility of using Commercial Off-the-Shelf (COTS) components, easy deployment, small size, low weight, low probability of interception and unnecessary frequency band allocation. On the other hand, complex signal processing techniques are required for targets' detection and tracking, due to the use of out-of-control IoOs and waveforms, designed for fulfilling quality requirements defined for the associated service.

Digital Video Broadcasting (DVB-T) [2]–[4], FM radio [5], [6], digital audio [7] or mobile communications systems [8], [9] have been analysed. DVB-T signals are of special relevance due to their good features in PR applications: high transmitted powers, high availability, known position and waveform, good autocorrelation characteristics, bandwidth around 8 MHz (with the possibility of using consecutive channels for increasing the system resolution), and spectral properties which are nearly independent of the signal content.

The bistatic/multiestatic geometry and the lack of control over the transmitter impose the use of reception systems composed of two channels: the reference one, to acquire the direct signal from the IoO, and the surveillance one to capture targets' echoes. In Figure 1, the basic scheme of a bistatic system is depicted: R_{T_i} is the target-to-transmitter distance, R_{R_i} is the target-to-receiver distance, L is the transmitter-to-receiver distance or baseline, β_i is the bistatic angle defined by R_{R_i} and R_{T_i}, and σ_{bis_i} is the Bistatic Radar Cross Section (BRCS), where $i \in \{a, b, c\}$ refers to *aeroplane*, *building* and *car*, respectively.

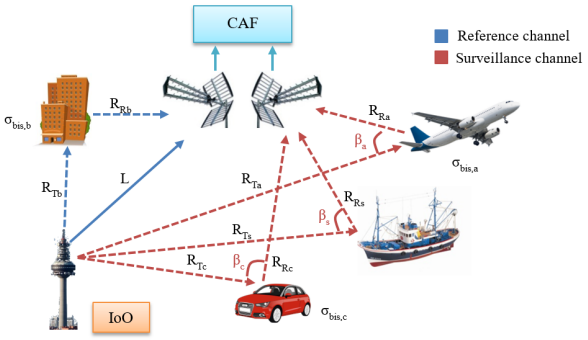

Fig. 1. Basic operating scheme of a Passive Bistatic Radar

To perform matching filtering, delayed and Doppler-shifted copies of the reference signal are correlated with the surveillance one to generate the Cross Ambiguity Function, CAF (1).

$$S^{CAF}[m,p] = \sum_{n=0}^{N-1} s^*_{ref}[n-m] \cdot s_{surv}[n] \cdot \exp^{-j2\pi \frac{p}{N} n} \quad (1)$$

- $N = T_{int} \cdot f_s$, is the number of samples, being T_{int} (s) the integration time, and f_s (Hz) the sampling frequency.
- m is the time bin associated with a delay $\tau_m = m/f_s$.
- p is the Doppler-shift corresponding to $f_{dop} = f_s\,(p/N)$.
- $s_{ref}[n]$ is the reference signal.
- $s_{surv}[n]$ is the surveillance signal.

Main interference sources are the Direct Path Interference (DPI) or direct IoO signal acquired by the surveillance antenna, IoO multipaths acquired by reference and surveillance antennas, other interfering IoOs belonging to the same Single Frequency Network (SFN), and the radar echoes generated by non-desired objects present in the coverage area (clutter).

ISBN 978-90-827970-1-5

If the IoO and the PR are stationary, and clutter sources are stationary or characterized by low Doppler shifts, although their effects spread along all the CAF domain, their maxima are located along the zero Doppler. In the literature, adaptive algorithms are usually applied before the CAF stage to reduce these non-desired signals and increase the detection performance of the system [10]–[12].

As an alternative approach, in [13], a statistical analysis of PR interferences was carried out considering the CAF ouput as the observation space, for the design of approximations to the optimum Neyman-Pearson (NP) detector based on statistical signal processing and artificial intelligence techniques. The CAF space was divided into different Doppler subregions to determine coherent and non-coherent clutter models for the intensity and the in-phase component of the CAF samples, respectively. Data acquired by a DVB-T passive radar demonstrator developed at the University of Alcalá [14], were used. Results demonstrated that the Gaussian model can be applied in areas of the CAF far from the zero Doppler, but for the areas close to the zero Doppler, Log-Normal, mixtures of Gammas, and mixtures of Gaussians were proposed for the intensity and the in-phase component, respectively.

In this paper, the most extended PR architecture based on adaptive filters for rejecting interferences, followed by the CAF and conventional Constant False Alarm Rate (CFAR) detectors is reconsidered. This solution assumes that most of the interference components are rejected by the adaptive filtering based pre-processing stage, and CFAR detectors operating on the CAF output are designed for Gaussian clutter residuals. To gain more insight about performance limitations of this solution and possible improvements to be achieved, specially for the detection of targets characterized by low Doppler shifts on the CAF, the statistical study performed in [13] is applied to the CAF generated after a pre-processing stage based on a Extensive Cancellation (ECA) algorithm, a solution widely used for the PR community [15], [16].

Results prove that when the CAF is generated from the ECA filtered surveillance signal, the areas close to the zero Doppler are not Gaussian distributed, so CFAR detectors based on Gaussian statistics used in the most PR receivers are not optimum. These results could be used for the design of improved detection schemes for this CAF area, where targets of great interest, such as drones, are expected.

II. Passive Radars Operating Principle

The operating principle of the PRs is based on the coherent processing of the IoO signal and the radar echoes generated by objects illuminated by the selected IoO. For each scatterer, the result of the CAF is the ambiguity function of the transmitted signal, scaled and shifted to be centred on the scatterer time delay and Doppler shift, which allows target detection and the estimation of its velocity and position (Figure 2).

The acquisition time, T_{acq}, is divided into Coherent Processing Intervals (CPI), of integration time T_{int} seconds, using a periodic pulse train with a selected Pulse Repetition Interval (PRI), Figure 3. A CAF is generated for each CPI,

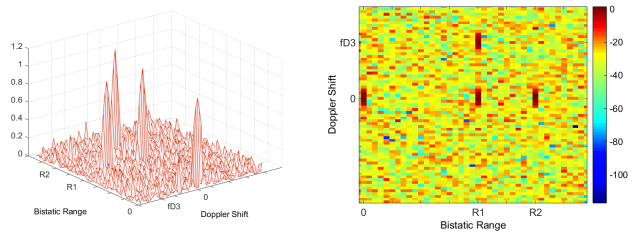

Fig. 2. Example of a CAF with 3 targets (two stationary targets at bistatic ranges $R1$ and $R2$, and one moving target located at position ($R1$, $fD3$)), and the DPI. Left: 3D CAF. Right: 2D CAF

and the detector transforms the CAF output to generate the detection matrix to be applied to the tracker in charge of associating targets' detections in successive CPIs for estimating their tracks (Figure 4).

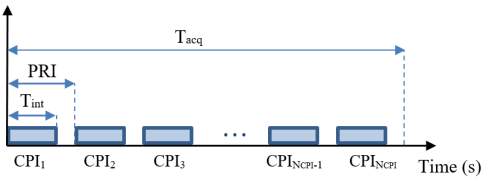

Fig. 3. Time processing parameters definition

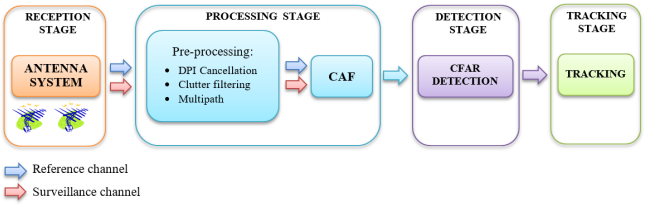

Fig. 4. Basic architecture of a Passive Radar

III. Extensive Cancellation (ECA) Filter

The ECA algorithm is one of the most extended solution for interference rejection in PR [10], [16]. The input and the desired signals are presented in (2), where $S_{ref}(n)$ and $S_{surv}(n)$ are the reference and surveillance signals, respectively. R extra samples of the reference signal are used, so the total number of acquired samples in the CPI is $N+R$.

$$\begin{aligned}\mathbf{S}_{ref} &= [S_{ref}(-R+1), ..., S_{ref}(0), S_{ref}(1), ...S_{ref}(N)] \\ \mathbf{S}_{surv} &= [S_{surv}(0), S_{surv}(1), ...S_{surv}(N)]\end{aligned} \tag{2}$$

The filtered signal vector, $\mathbf{S}_{surv_{fil}} = [S_{surv_{fil}}(0), S_{surv_{fil}}(1), ...S_{surv_{fil}}(N)]$, is calculated as the projection of the desired input vector $\mathbf{S}_{surv}$ defined in (2) on the orthogonal subspace to the zero Doppler interference subspace. The projection matrix, $\mathbf{P}_0$, is calculated as is described in (3), where the operator $\mathbf{D}$ applies a one lag delay, and $\mathbf{\Lambda}_p$ is a diagonal matrix that applies the phase shift corresponding to the p-th Doppler bin [10].

ISBN 978-90-827970-1-5 © EURASIP 2018

$$\begin{aligned}\mathbf{S}_{surv_{fil}} &= [\mathbf{I}_N - \mathbf{X}(\mathbf{X}^H\mathbf{X})^{-1}\mathbf{X}^H]\mathbf{S}_{surv} \\ \mathbf{X} &= \mathbf{B}[\mathbf{\Lambda}_{-p}\mathbf{S}_{ref}, ..., \mathbf{S}_{ref}, ..., \mathbf{\Lambda}_p\mathbf{S}_{ref}] \\ \mathbf{S}_{ref} &= [\mathbf{S}_{ref}\mathbf{D}\mathbf{S}_{ref}...\mathbf{D}^{(K-1)}\mathbf{S}_{ref}]\end{aligned} \quad (3)$$

This solution uses a unique filter weight vector for each CPI. The associated computational cost is defined by the CPI duration time and the clutter subspace dimension. In PR systems, this computational cost is higher due to the long processing times required to increase the integration gain.

IV. Clutter modeling

The radar scenario is the same as that described in [14] and [13]. In Figure 5, the view from the surveillance antenna is shown, together with the CAF generated without any pre-processing stage and the combination of the ECA filter and the CAF. As the ECA filter coefficients' vector is not normalized to unit energy, the background level is higher in the second CAF (calculated from the output of the ECA filter). However, the relevant magnitude from the detection point of view is the different between the zero Doppler line level and the background level, which is significantly higher when the ECA filter is applied, proving its capability for rejecting stationary interferences.

As Doppler resolution is a function of the integration time, two values ($T_{int} = 250$ ms and $T_{int} = 500$ ms) were considered in [13] (Doppler resolutions equal to 4 Hz and 2 Hz, respectively). For saving space, in this paper, the study for $T_{int} = 250$ ms is reconsidered, for the clutter statistical analysis of the CAF and the combination of an ECA filter and the CAF.

In the left image of Figure 5, a parking area with trees and three Big Buildings (BBs) were identified. Main PR parameters were: central frequency variable from 450MHz up to 850MHz, signal bandwidth 25MHz, and continuous acquisition time up to 40 s. The measurement campaign was carried out controlling that there was not any moving target during system operation. For $T_{int} = 250$ ms, CAF subregions are the following:

- Areas far from the zero Doppler: 1A $[-799; -550]Hz$, and 1B $[550; 799]Hz$.
- Areas where aircrafts flying at low altitudes could be detected: 2A $(-550; -300]Hz$, and 2B $[300; 550)Hz$.
- Areas where terrestrial vehicles are expected [14]: 3A $(-300; -40]Hz$, 3B $[40; 300)Hz$, and 4 $(-40; 40)Hz$. Area 4 is of special interest because it concentrates ground clutter highest contributions.

In this paper, the clutter characterization is carried out using the statistical analysis techniques detailed in [13]: estimating the Empirical Probability Density Function (EPDF) and Empirical Cumulative Distribution Function (ECDF), applying two-sample goodness-of-fit tests (Kolmogorov-Smirnov (KS-test2) and Crámer-von-Mises (CM-test2) tests) to assess the suitability of several theoretical distributions (if the $p - value$ is less than the chosen significance level, α, the selected theoretical distribution may be rejected); and analysing the in-phase (I) and in-quadrature (Q) components obtaining the skewness (γ_3) and excess kurtosis ($\gamma_{4,exc}$) parameters. The theoretical distributions selected in [13] are also considered: Exponential (E), Weibull (W), K-distribution (K), Log-Normal (LN), Gamma (Γ), and Gamma Mixture Distribution (ΓMD) for modeling the intensity; and Normal (N), Logistic (LG) and Gaussian Mixture Distribution (GMD) for characterizing the real and imaginary parts. Due to I and Q components were identically distributed, and the PDF of data amplitude can be obtained from the PDF of its intensity, only the results related to the I component and the intensity are presented.

V. Statistical Analysis Results

Results presented in [13] proved that a Gaussian clutter model could be assumed for regions $i - A$ and $i - B$, $i = 1, 2, 3$ if no pre-processing stage that could alter clutter statistics of the CAF was applied. In this paper, a processing scheme composed of an ECA filter followed by the CAF was considered. Statistical analysis results obtained assuming $\alpha = 5\%$ confirm that similar clutter characterization was obtained for regions $i - A$ and $i - B$, $i = 1, 2, 3$:

- The intensity was exponentially distributed.
- Skewness and excess kurtosis values of I and Q components prove the suitability of the Gaussian clutter model.

Figure 6 shows the estimated standard deviations of the Gaussians distributions for the different regions when no pre-filtering stage is applied, and when an ECA filter is used. For both cases, statistical parameters were similar in regions i-A and i-B ($i = 1, 2, 3$). However, the standard deviation values obtained for the ECA case are higher than those obtained without pre-filtering stage.

In region 4, all considered distributions were rejected, as is confirmed in Table I, where the KS and CM distances, and the $p-value$ for the CM-test2 in the ECA case are summarized. In Table II, the in-phase and in-quadrature analysis results show skewness and excess kurtosis estimated values quite different to those expected in a Gaussian clutter model. Higher excess kurtosis values were obtained for the no pre-filtering case.

An exhaustive analysis was performed in region 4 dividing it into different sub-regions:

- Intervals (Hz): [-42,-14), [22,30) and [30,42).
- Doppler lines (Hz): [-14,-10); [-10,-6); [-6,-2); [-2, 2); [2, 6); [6, 10); [10, 14); [14, 18) and [18, 22);

In Table III, the theoretical distributions that fulfil the goodness-of-fit tests, and the associated $p - values$ of the CM-test2 for the selected sub-regions are summarized. Mixtures of Gammas and mixtures of Gaussians are suitable to model the intensity and the I component, respectively. In [13], when no pre-filtering stage was applied, any of the considered distributions passed the test to characterize the intensity of the zero Doppler line, selecting the Log-Normal distribution due to its lower associated error. In the ECA filter case, two mixture of Gammas and Gaussians are proposed to model the

ISBN 978-90-827970-1-5

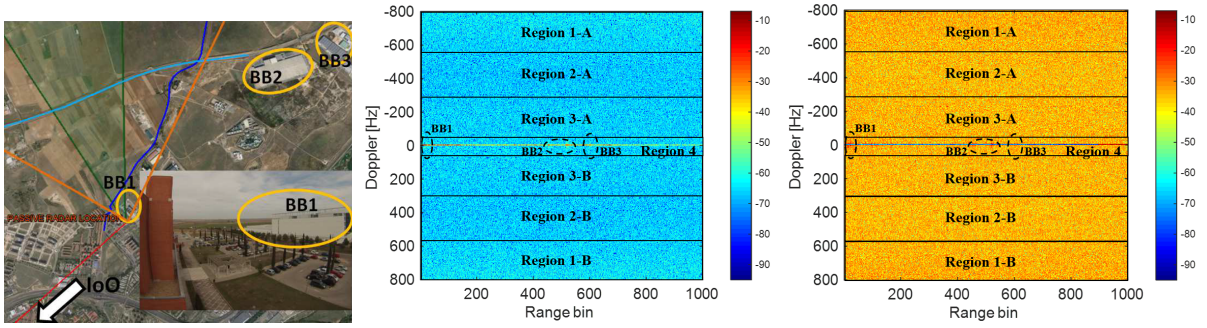

Fig. 5. PR surveillance antenna view (left), CAF intensity without pre-processing (centre), ECA and CAF stage (right). Each CAF matrix is composed of $1,000$ range bins, covering a distance of 9.450 km along the pointing direction. Doppler ranges from -799.744Hz to 799.744Hz

TABLE I
GOODNESS-OF-FIT TEST DISTANCES AND $p-value$ FOR CM-TEST2 WITH $\alpha = 0.05$. REGION 4 FOR THE ECA FILTER CASE

Intensity															I component					
E			W			K			LN			Γ			N			LG		
d_{KS}	d_{CM}	p_{CM}	d_{KS}	d_{CM}	p_{CM}	d_{KS}	d_{CM}	p_{CM}	d_{KS}	d_{CM}	p_{CM}	d_{KS}	d_{CM}	p_{CM}	d_{KS}	d_{CM}	p_{CM}	d_{KS}	d_{CM}	p_{CM}
0.11	**63**	**0**	**0.08**	**23**	**0**	**0.92**	**3002**	**0**	**0.18**	**117**	**0**	**0.08**	**28**	**0**	**0.05**	**11**	**0**	**0.03**	**0.87**	**0**

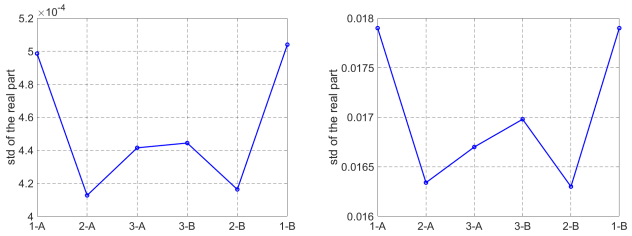

(a) without pre-filtering stage (b) with ECA filter

Fig. 6. Estimated standard deviations of the Gaussians distributions for regions $i-A$ and $i-B$, $i=1,2,3$

TABLE II
SKEWNESS AND EXCESS KURTOSIS VALUES ESTIMATED FOR THE I AND Q COMPONENTS IN REGION 4

	Without pre-filtering		**ECA filtering**	
	I	*Q*	*I*	*Q*
γ_3	-2.342	-19.740	4.855	-1.036
$\gamma_{4,exc}$	469.957	$1.776 \cdot 10^3$	201.47	30.909

intensity and the I component, respectively. In Figure 7, the ECDF and some theoretical CDFs are depicted for the zero Doppler line when the ECA filter was applied, proving the rejection of the Exponential and Normal distributions due to their higher associated error.

Next to the zero Doppler line ($f_d \in [-6,-2)$ Hz and $f_d \in [2,6)$ Hz), a higher number of ΓMD and GMD are required to model the intensity and the I component, respectively, in the ECA case compared to the no pre-filtering one (marked in blue in Table III). In Figure 8, ECDFs are compared to theoretical models for $f_d \in [-6,-2)$ Hz and $f_d \in [2,6)$ Hz, where the differences between the ECDFs and the 2-ΓMD and 2-GMD are observed. Figure 9 shows the variation of the

TABLE III
THEORETICAL MODELS THAT FULFIL THE GOODNESS-OF-FIT TESTS AND $p-value$ FOR THE CM-TEST2 WITH $\alpha = 0.05$. REGION 4

f_d (Hz)	**Without pre-filtering**				**ECA filtering**			
	Intensity		*Real part*		*Intensity*		*Real part*	
	PDF	p-value	PDF	p-value	PDF	p-value	PDF	p-value
$[-42,-14)$	E	0.522	N	0.525	E	0.586	N	0.854
$[-14,-10)$	2-ΓMD	0.819	2-GMD	0.681	2-ΓMD	0.693	2-GMD	0.174
$[-10,-6)$	2-ΓMD	0.649	2-GMD	0.615	2-ΓMD	0.694	2-GMD	0.908
$[-6,-2)$	2-ΓMD	0.369	2-GMD	0.376	3-ΓMD	0.967	3-GMD	0.365
$[-2,2)$	LN	1	4-GMD	0.11	2-ΓMD	0.926	2-GMD	0.165
$[2,6)$	2-ΓMD	0.251	2-GMD	0.101	3-ΓMD	0.731	3-GMD	0.425
$[6,10)$	2-ΓMD	0.602	2-GMD	0.511	2-ΓMD	0.134	2-GMD	0.822
$[10,14)$	2-ΓMD	0.635	2-GMD	0.75	2-ΓMD	0.504	2-GMD	0.941
$[14,18)$	2-ΓMD	0.433	2-GMD	0.173	2-ΓMD	0.121	2-GMD	0.088
$[18,22)$	2-ΓMD	0.102	2-GMD	0.095	2-ΓMD	0.413	2-GMD	0.934
$[22,30)$					E	0.631	N	0.855
$[30,42)$	E	0.454	N	0.257				

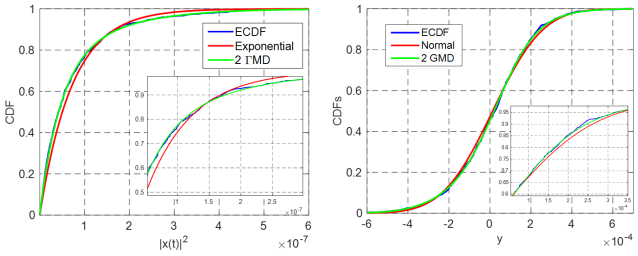

(a) Intensity (b) Real Part

Fig. 7. CDFs for the zero Doppler line with ECA filter

GMD parameters throughout the defined Doppler subregions.

VI. CONCLUSION

In this paper, a statistical analysis of bistatic radar clutter in terrestrial scenarios was carried out. The effects on the ground clutter characterization of one of the most extended PR architecture based on ECA filter for rejecting interference

ISBN 978-90-827970-1-5 © EURASIP 2018

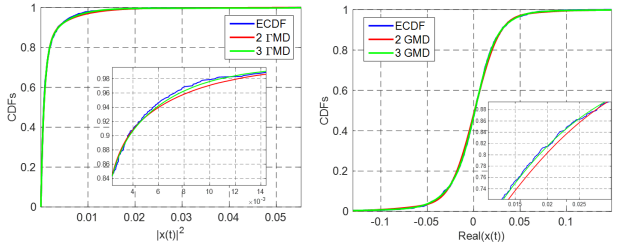

(a) $f_d \in [-6, -2)$ Hz: Intensity (left), I component (right)

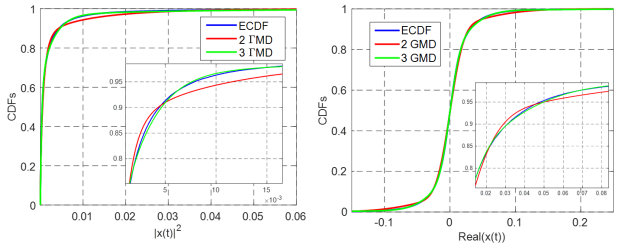

(b) $f_d \in [2, 6)$ Hz: Intensity (left), I component (right)

Fig. 8. CDFs for region 4 with ECA filter: $f_d \in [-6, -2)$ Hz (top); $f_d \in [2, 6)$ Hz (bottom)

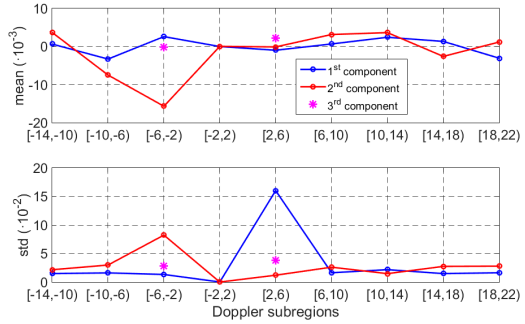

Fig. 9. $GMDs$ parameters for the I component for the ECA filter case

components followed by the CAF were studied. Real radar data acquired by the technological demonstrator IDEPAR, a multichannel DVB-T based PR system, were analyzed. The selected scenario was a semi-urban environment characterized by the presence of big buildings, that were expected to generate strong radar returns, and parking areas with trees.

A methodology based on the analysis of the output of the CAF is proposed. All radar returns spread throughout the whole delay-Doppler plane defined by the CAF, which justifies the necessity of performing a statistical analysis throughout all CAF delay-range and Doppler shift space. The statistical characterization of the radar data was performed estimating the ECDF, and applying goodness-of-fit tests to assess the suitability of several theoretical distributions. Skewness and kurtosis parameters were also calculated to analyse the in-phase and quadrature components.

As in the no pre-filtering case, results proved that a Gaussian clutter model could be assumed for absolute Doppler shifts higher than 40Hz, and a non-homogeneous characterization was required in the region centred on the zero Doppler when an ECA filter was applied. Compound models composed of mixtures of Gamma and Gaussian PDFs were proposed for modelling the intensity and the real and imaginary parts of the data, respectively.

CFAR detectors designed assuming a Gaussian clutter model are usually implemented in PR systems. Taking into account the results obtained in this paper, these solutions are not optimum in the region centred on the zero Doppler shift. Improved detection schemes based on the proposed statistical models could be designed for this CAF area, where targets of great interest, such as drones, are expected.

ACKNOWLEDGMENT

This work has been partially funded by the Spanish Ministerio de Economía, Industria y Competitividad (project TEC2015-71148-R), the European FP7 SCOUT Project (Grant Agreement n. 607019), and by the University of Alcalá (project CCGP2017-EXP/056).

REFERENCES

[1] "IEEE Standard for Radar Definitions," *IEEE Std 686-2017 (Revision of IEEE Std 686-2008)*, pp. 1–54, 2017.

[2] R. Saini and M. Cherniakov, "DTV signal ambiguity function analysis for radar applications," in *IEE Proc. on Radar, Sonar and Navigation*, vol. 152, no. 3, 2005, pp. 133–142.

[3] J.-L. Bárcena-Humanes, J. Martín-Nicolás, C. Sols-Carpintero, P. Jarabo-Amores, M. Rosa-Zurera, and D. Mata-Moya, "DVB-T ambiguity peaks reduction in passive radar applications based on signal reconstruction," in *44th European Microw. Conf.*, 2014, pp. 1900–1903.

[4] D. W. O'Hagan and et al., "Wideband antenna array for digital video broadcast terrestrial-based passive bistatic radar applications," *IET Radar, Sonar Navigation*, vol. 8, no. 2, pp. 106–113, 2014.

[5] P. E. Howland and et al., "FM radio based bistatic radar," in *IEE Proc. on Radar, Sonar and Nav.*, vol. 152, no. 3, 2005, pp. 107–115.

[6] M. Malanowski, K. Kulpa, and J. Misjurewicz, "PaRaDe - Passive Radar Demostrator family development at Warsaw University of Technology," *Microwaves, Radar and Remote Sensing Symposium*, pp. 75–78, 2008.

[7] C. Coleman and et al., "A practical bistatic passive radar system for use with DAB and DRM illuminators," *IEEE Radar Conf.*, pp. 1–6, 2008.

[8] R. Zemmari, U. Nickel, and W. Wirth, "GSM Passive Radar for medium range surveillance," *EuRAD*, pp. 49–52, 2009.

[9] D. Petri, A. Capria, M. Martorella, and F. Berizzi, "Ambiguity function study for UMTS Passive Radar," *EuRAD*, pp. 41–44, 2009.

[10] F. Colone, R. Cardinali, and P. Lombardo, "Cancellation of clutter and multipath in passive radar using a sequential approach," in *IEEE Conf. on Radar*, 2006, pp. 1–7.

[11] R. Saini, M. Cherniakov, and V. Lenive, "Direct path interference suppression in bistatic system: DTV based radar," in *Radar Conference, 2003. Proceedings of the International*, Sept 2003, pp. 309–314.

[12] D. Wu and et al., "Improved LMS algorithm and its application in direct path and multipath cancellation for passive radar," in *IEEE Int. Conf. on Comm. Technology*, 2012, pp. 1301–1305.

[13] N. del Rey-Maestre, M.-P. Jarabo-Amores, D. Mata-Moya, J.-L. Bárcena-Humanes, and P.-J. Gomez-del Hoyo, "Machine learning techniques for coherent CFAR detection based on statistical modeling of UHF passive ground clutter," *IEEE Journal of Selected Topics in Signal Processing*, vol. PP, no. 99, pp. 1–15, 2017.

[14] M.-P. Jarabo-Amores, J.-L. Bárcena-Humanes, P.-J. Gomez-del Hoyo, N. del Rey-Maestre, D. Juara-Casero, F.-J. Gaitán, and D. Mata-Moya, "IDEPAR: a multichannel digital video broadcasting-terrestrial passive radar technological demonstrator in terrestrial radar scenarios," *IET Radar, Sonar and Nav.*, pp. 1–9, 2016.

[15] F. Colone and et al., "A multistage processing algorithm for disturbance removal and target detection in passive bistatic radar," *IEEE Trans. on Aerospace and Electronic Systems*, vol. 45, no. 2, pp. 698–722, 2009.

[16] R. Cardinali, F. Colone, C. Ferretti, and P. Lombardo, "Comparison of clutter and multipath cancellation techniques for passive radar," in *IEEE Radar Conf.*, vol. 1, 2007, pp. 469–474.